AIAA JOURNAL
Vol. 38, No. 10, October 2000

Interference Effects During Burning of Tandem Porous Spheres in Mixed Convective Environment

P. Balakrishnan,* T. Sundararajan,† and R. Natarajan‡
Indian Institute of Technology, Madras, Chennai 600 036, India

The interference effects during the burning of a binary tandem droplet array in a mixed convective environment have been studied both theoretically and experimentally for the upward airflow configuration. In the theoretical model, the flow and transport equations have been solved subject to the assumptions of constant properties (except for density) and infinite rate kinetics, by the use of the finite element method. The gas density has been treated as a variable, only for evaluating the buoyancy force contribution, and it has been determined through the ideal gas mixture assumption. A porous-sphere facility has been employed for simulating experimentally the burning characteristics of a fuel droplet array with fixed separation distance. The measured mass burning rates for both the spheres and the observed flame shapes are in excellent agreement with the corresponding theoretical predictions. The burning rate of the rear droplet is considerably less than that of the front droplet or an isolated droplet, for smaller separation distances. For larger separation distances, the burning rate of the rear droplet is of the same order as the front droplet, and it is sometimes even larger than that of the isolated droplet. The rate of burning of the front droplet mildly varies with separation distance, and it is approximately equal to that of an isolated droplet. The flame of a tandem binary droplet system is observed to be pushed away from the axis due to the presence of the second droplet.

Nomenclature

C_p	= specific heat
d	= droplet diameter
Fr	= Froude number, $u_\infty/(gd)^{1/2}$
Gr	= Grashof number, $g\beta(T_f - T_\infty)d^3/\nu^2$
g	= gravitational acceleration
h_{fg}	= enthalpy of vaporization
M_f, M_o	= molecular weight of fuel and oxygen
M_p	= molecular weight of the products
Nu	= Nusselt number, $[k_s d/k_\infty(T_\infty - T_s)](\partial T/\partial r)_s$
Pe	= Peclet number, $u_\infty d/D$
p	= pressure
R	= gas constant
Re	= Reynolds number, $\rho u_\infty d/\mu$
R_u	= universal gas constant
r	= radial coordinate
T	= temperature
T_{ad}	= adiabatic flame temperature
T_b	= boiling point temperature of the fuel
T_0	= standard temperature, 298.16 K
T_∞	= ambient temperature
u	= velocity in the axial direction
u_∞	= farstream air velocity
v	= velocity in the radial direction
Y_f, Y_o	= mass fraction of fuel and oxygen
$Y_{o,\infty}$	= ambient oxygen mass fraction
z	= axial coordinate
β_1, β_2	= Shvab–Zeldovich variables
ν_f, ν_o	= stoichiometric coefficients of fuel and oxygen
ρ	= density

I. Introduction

INTERFERENCE caused by neighboring droplets significantly modifies the combustion and flow features of a fuel droplet. As a first step toward understanding the complex features of spray combustion, it would be useful to develop data on the combustion of known droplet array configurations. In the present study, a simple theoretical model has been developed for analyzing the interference effects for a vertical array of two droplets in a mixed convective environment. The model has been validated with data from porous-sphere experiments, both with regard to the burning rate and flame shape predictions.

Comprehensive surveys of the available literature on droplet interaction effects have been provided in the recent review papers by Annamalai and Ryan[1] and Umemura.[2] Mikami et al.[3] studied the droplet interference effects for a wide range of initial separation distances between two droplets. Theoretical studies on interference effects during the evaporation of fuel droplets have been carried out by Labowsky,[4,5] Brzustowski et al.,[6] Umemura et al.,[7] and Williams et al.[8] Marberry et al.[9] showed that particle interactions are strong functions of their sizes, number density, and array geometry. Shuen[10] studied the effects of droplet interaction on evaporation and combustion of a planar droplet array. Parameters investigated include the droplet spacing, droplet Reynolds number, oxygen concentration of approaching stream, and the fuel type. The effects of particle interactions on evaporation and combustion have also been studied by Tal et al.,[11] Sirignano,[12] Raju and Sirignano,[13] and Umemura.[14] Tsai and Sterling[15] studied the combustion of a linear droplet array in convective flow. The results indicate that the droplet burning behavior is affected by Reynolds number, droplet spacing, and relative location of droplets in the array. Recently, Sivasankaran et al.[16] analyzed the interference effects between two burning spheres in a quiescent atmosphere, using the finite element method. The transient evolution of droplet sizes and positions during the combustion of a monodisperse droplet array have been studied experimentally and theoretically by Roth et al.[17] The flow features of noncombusting droplet streams have been studied by Nguyen et al.[18]

A majority of the earlier theoretical studies dealt with multidroplet evaporation without combustion or combustion in the absence of flow. During the combustion of large fuel droplets, natural convective effects may become important, in addition to forced convective effects. The theoretical model developed in the present study highlights the individual and combined effects of natural and forced convective flowfields on the combustion of a vertical droplet array. It employs the thin flame formulation with appropriately averaged properties, except for gas density variation in the buoyancy force term. Experimental investigations for tandem droplet combustion have also been carried out using the porous-sphere technique.

Received 29 June 1999; revision received 11 February 2000; accepted for publication 7 March 2000.

*Research Scholar, Department of Mechanical Engineering.
†Professor of Mechanical Engineering, Department of Mechanical Engineering.
‡Director and Professor of Mechanical Engineering; nataraj@shiva.iitm.ernet.in.

II. Governing Equations and Boundary Conditions

It has been generally believed that constant property models can not accurately predict all of the important characteristics of droplet combustion, such as burning rate, flame shape, and flame temperature.[19,20] For this reason, in some recent studies,[15] detailed property variations and finite rate kinetics have been taken into account. However, the present study shows that the most significant correction to the constant property model is the density variation in the buoyancy force term, for droplet Reynolds number in the range of $\mathcal{O}(10)$. When gas density variation in this term is taken into account appropriately (by an ideal gas mixture assumption), the predictions of the simplified model agree remarkably well with the experimental data as well as the predictions of more elaborate models. Therefore, the following usual simplifying assumptions have been invoked in the present model: infinite rate kinetics, quasi-steady burning, constant properties, axisymmetric flow, unit Lewis number for all species, and a binary mixture of fuel and products or oxygen and products existing on either side of the flame. The justification for some of the critical assumptions stated is provided elsewhere in the text.

Subject to these assumptions, the nondimensional governing equations can be written in terms of the Shvab–Zeldovich variables (Fig. 1) as follows:

1) The continuity equation is

$$\frac{\partial u}{\partial z} + \frac{\partial v}{\partial r} + \frac{v}{r} = 0 \tag{1}$$

where u and v denote the velocity components in the axial and radial directions, respectively.

2) The z-momentum equation is

$$u\frac{\partial u}{\partial z} + v\frac{\partial u}{\partial r} = -\frac{\partial p}{\partial z} + \frac{1}{Re}\nabla^2 u + \frac{1}{Fr^2}\left(\frac{\rho_\infty}{\rho} - 1\right) \tag{2}$$

Here, ρ is the local density, $Re = \rho u_\infty d/\mu$ is the Reynolds number, d is the diameter of the bigger droplet in the case of unequal droplets, and $Fr = u_\infty (gd)^{1/2}$ is the Froude number. The local gas density has been evaluated as

$$\rho = \sum \frac{p}{R_i T} Y_i$$

3) The r-momentum equation is

$$u\frac{\partial v}{\partial z} + v\frac{\partial v}{\partial r} = -\frac{\partial p}{\partial r} + \frac{1}{Re}\left(\nabla^2 v - \frac{v}{r^2}\right) \tag{3}$$

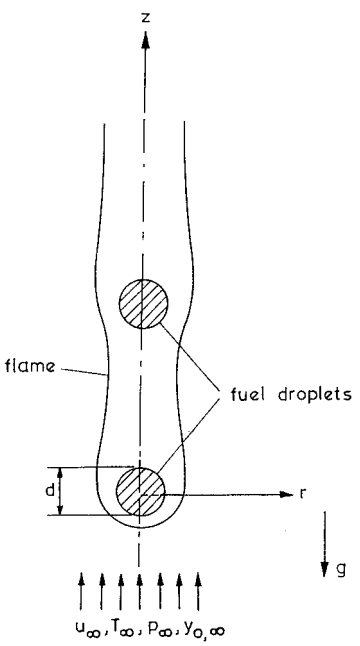

Fig. 1 Two tandem droplets burning in upward air flow configuration.

4) The Shvab–Zeldovich transport equations are

$$u\frac{\partial \beta_1}{\partial z} + v\frac{\partial \beta_1}{\partial r} = \frac{1}{Pe}\nabla^2 \beta_1 \tag{4}$$

$$u\frac{\partial \beta_2}{\partial z} + v\frac{\partial \beta_2}{\partial r} = \frac{1}{Pe}\nabla^2 \beta_2 \tag{5}$$

where

$$\beta_1 = \frac{M_{f,o} C_p (T - T_0)}{\Delta H \nu_f M_f} + \frac{M_{f,o} Y_o}{\nu_o M_o}, \qquad \beta_2 = \frac{M_{f,o} Y_f}{\nu_f M_f} - \frac{M_{f,o} Y_o}{\nu_o M_o}$$

and $M_{f,o} = \nu_f M_f + \nu_o M_o$. Also, ΔH is the enthalpy of combustion, ν_f and ν_o are the stoichiometric coefficients of fuel and oxygen, M_f and M_o are the molecular weights of fuel and oxygen, T is the temperature, and T_0 is the standard reference temperature (=298.16 K) for enthalpy calculations.

In fact, the equations for Shvab–Zeldovich variables (4) and (5) have been derived by combining the energy equation and the transport equations for the fuel and oxidizer species.[21] The corresponding boundary conditions for the problem (Fig. 1) are as follows:

1) At farstream,

$$u = u_\infty, \qquad v = 0$$

$$\beta_1 = \beta_{1,\infty} = \frac{M_{f,o} C_p (T_\infty - T_0)}{\nabla H \nu_f M_f} + \frac{M_{f,o} Y_{o,\infty}}{\nu_o M_o}$$

$$\beta_2 = \beta_{2,\infty} = -\frac{M_{f,o} Y_{o,\infty}}{\nu_o M_o} \tag{6}$$

2) At the flow axis,

$$\frac{\partial u}{\partial r} = 0, \qquad v = 0, \qquad \frac{\partial p}{\partial r} = 0, \qquad \frac{\partial \beta_1}{\partial r} = 0, \qquad \frac{\partial \beta_2}{\partial r} = 0 \tag{7}$$

3) On the surfaces of the droplets the balance of heat and species flux gives the following form of gradient boundary condition:

$$\frac{\partial \beta_2}{\partial n} = \frac{\Delta H}{h_{fg}}\left(\frac{\beta_2 \nu_f M_f}{M_{f,o}} - 1\right)\frac{\partial \beta_1}{\partial n} \tag{8}$$

where n is the local normal coordinate to the droplet surface. Using the relationship between fuel vapor fraction at the surface and the droplet temperature (via the Clausius Clapeyron equation), one can obtain

$$\beta_1 = \frac{M_{f,o} C_p}{\Delta H \nu_f M_f}\left(1 \Big/ \left\{\frac{R}{h_{fg}} \ell n\left[\left(\frac{M_{f,o}}{\nu_f M_f \beta_2} - 1\right)\frac{M_f}{M_p} + 1\right] + \frac{1}{T_b}\right\} - T_0\right) \tag{9}$$

The tangential velocity is approximated as zero, and the normal velocity is calculated from

$$v_n = \frac{1}{Pe}\frac{\Delta H}{h_{fg}}\frac{\nu_f M_f}{M_{f,o}}\frac{\partial \beta_1}{\partial n} \tag{10}$$

where v_n is the normal gas-phase velocity at the surface due to evaporation.

The average properties for the mixture have been evaluated as follows: For the mixture inside the flame, the average temperature is taken to be $(T_b + T_{ad})/2$, and the reference concentration is taken as the average between pure fuel vapor (at drop surface) and complete combustion products (at flame surface). For the mixture outside the flame, the reference temperature is taken as the average between T_∞ and T_{ad}, whereas the concentration is averaged between the ambient air and the product composition at flame surface. The overall mixture properties are taken as the mean between the average properties for the two zones. Typical properties employed in the computations are listed in Table 1.

Table 1 Typical properties employed in computations[a]

Property	Value
Enthalpy of combustion, ΔH, kJ/kg	21,093
Adiabatic flame temperature, K	2,333
Mixture specific heat, kJ/kg · K	1.58395
Ratio of molecular weights, M_f / M_p	1.16306
Enthalpy of vaporization, h_{fg}, kJ/kg	1,101
Normal boiling point, T_b, K	337.85
Gas constant, R, kJ/kg · K	0.2594
Molecular weight of fuel, M_f, kg/kmol	32.042
Stoichiometric coefficient of fuel, ν_f	1.0
Stoichiometric coefficient of oxygen, ν_o	1.5
Kinematic viscosity, ν, m^2/s	177×10^{-6}

[a] $p_\infty = 1$ bar, $T_\infty = 300$ K, and $Y_{o,\infty} = 0.23$.

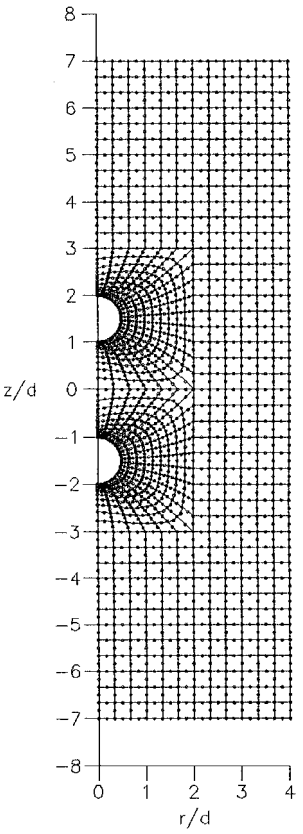

Fig. 2 Finite element grid.

III. Numerical Solution Procedure

The Galerkin's weighted residual procedure has been applied to solve the preceding set of equations. Eight-noded isoparametric elements have been employed as shown in Fig. 2. Quadratic interpolation has been used for the velocity components and the Shvab–Zeldovich variables, giving rise to interpolation expressions of the form

$$u = \sum_{i=1}^{8} N_i u_i, \qquad v = \sum_{i=1}^{8} N_i v_i$$

$$\beta_1 = \sum_{i=1}^{8} N_i \beta_{1,i}, \qquad \beta_2 = \sum_{i=1}^{8} N_i \beta_{2,i}$$

within each element. The pressure has been interpolated using only the corner nodes of each element through the expression

$$p = \sum_{i=1}^{4} M_i p_i$$

to avoid spurious numerical oscillations in the flow solutions.[22] In the preceding expressions, N_i and M_i are biquadratic and bilinear shape functions, respectively. After we substitute for the interpolation expressions for each solution variable, the weighted residual forms of the governing equations can be converted into elemental matrix contributions. By assembling all of the elemental contributions, the final system of nonlinear algebraic equations can be obtained. The frontal technique has been applied for iteratively solving these nonlinear equations.[22] Iterations are continued until all of the solution variables converge to four significant digits.

IV. Experimental Procedure

The overall experimental setup consisting of porous alundum spheres, fuel feed, and airflow system, is shown in Fig. 3. The porous spheres have been prepared by mixing aluminium oxide with fire clay, silica gel, and water in suitable proportions, then drying the wet spheres in air initially and subsequently baking them at 1000 K for about 5 h. A stainless steel hypodermic needle of 1.2-mm diam has been used to support the alundum spheres. The other end of the needle is connected to a glass syringe and an infusion pump, for supplying the fuel. Proper distribution of fuel over the surface of the porous sphere is ensured by drilling radial holes of 0.4 mm diam at the end of the hypodermic needle and verifying that the entire surface of the sphere is wetted when fuel is supplied by the pump. The volume flow rate from the syringe is directly shown by the digital system provided in the infusion pump. The spheres are supported above a vertical wind tunnel with a settling chamber of 200-mm diam and fitted with a Mache–Hebra nozzle of 75-mm exit diameter. The supply air line is fitted with a calibrated orifice plate to measure the flow rate.

Mass burning rate is measured by noting the fuel flow rate (in milliliters per hour) from the syringe, when any further increase in flow rate will result in the dripping of unburnt fuel from the burning droplet. The spheres were arranged one above the other with the desired separation distance, and the vertical air flow velocity was varied as per requirement. Both equal and unequal droplets were considered in the present study. Experiments have been conducted in the range of sphere diameter $d = 8$ and 16 mm and freestream velocity $\mu_\infty = 0.4$ and 0.8 m/s, with methanol as the fuel. Although the sizes of the spheres employed here are much larger than those encountered in a typical droplet spray, the burning rate results have been presented in the form of a dimensionless correlation to be of general use. Also, the inter-droplet spacings have been maintained constant with respect to time in both the experimental and theoretical parts of the present study, in contrast to the actual fuel sprays for which the spacing will change dynamically with time. Yet, the results of the present study could provide some basic insight before we study problems of practical interest.

The ranges of errors in the primary measurements are: mass burning rate, ±1%; sphere diameter, ±0.25%; and air velocity, ±1.5%.

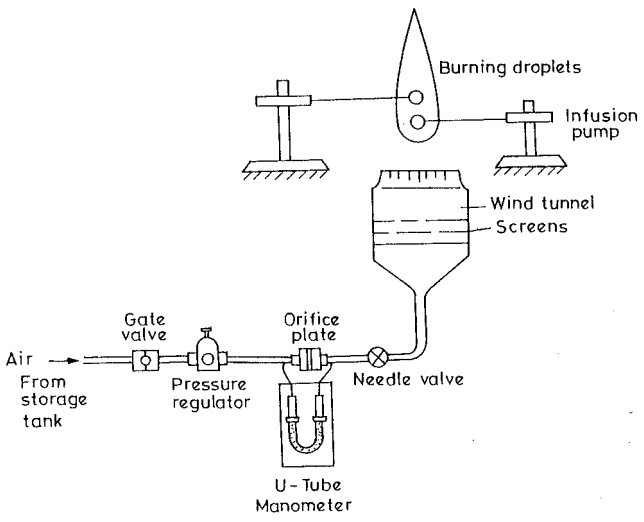

Fig. 3 Schematic diagram of the experimental setup.

V. Results and Discussion

A. Model Validation

Tsai and Sterling[15] simulated the combustion process of a rectilinear array of three droplets by employing a one-step, finite rate kinetic model and numerically solved the governing transport equations using an elliptical grid. In the present work, as shown in Fig. 2 for a binary tandem droplet arrangement, the computational domain is discretized into small eight-noded quadrilateral elements with the transfinite interpolation procedure for grid generation. Even though different types of grids have been employed in the two studies, Figs. 4 and 5 illustrate that the results of local Nusselt number and isotherms predicted by the present model closely match with those of Tsai and Sterling.[15] A general model with finite rate kinetics and detailed property variations was considered by Tsai and Sterling,[15] whereas the present study has employed the assumptions of constant physical properties and infinite rate kinetics. Still, good agreement has been observed between the two sets of results because of the following reasons. For diffusion flame combustion, convective-diffusion processes are primarily rate controlling and chemical kinetics has only a minor role to play. [For the ranges of conditions considered in the present study, the diffusion timescale is of the order of 1 s, whereas those of convection and kinetics can be estimated to be one and three orders faster than the diffusion scale, that is, $\mathcal{O}(10^{-1})$ and $\mathcal{O}(10^{-3})$ seconds, respectively.] As regards property variations, suitably averaged properties have been employed as suggested by Law and Law.[20] The numerical predictions illustrate that the most important property variation to be included in the analysis is that of mixture density. When the ideal gas mixture rule is employed for evaluating local gas density in the buoyancy term, the predictions agree quite well. Instead, if a constant density value was employed and the free convection effects were neglected, the predicted burning rate differed by as much as 25% from the experimentally measured value. The results also illustrate that the local Nusselt number variation of the first droplet is virtually the same as that of an isolated droplet for the spacing considered.

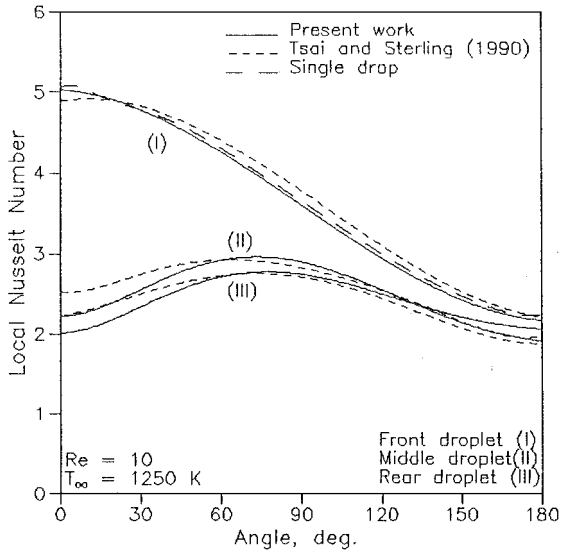

Fig. 4 Variation of local Nusselt number with angle for burning of three droplets.

Figure 6 illustrates that the flame shape predicted by the present model is also very close to that obtained from the experiment. The experimental flame shape has been obtained by identifying the maximum luminosity surface from a flame photograph, with the help of a digital image processing system. Law and Law[20] showed that a reasonable agreement for the flame shape during spherical combustion (in the absence of convection) can be achieved only if different Lewis number ($Le \neq 1$) values are used for the inner and outer regions of the flame. However, for the conditions encountered in the present study, the flame shape is also primarily governed by the convective flow pattern around the droplets as shown in the comparison of the time scales for $Re = \mathcal{O}(10)$. Therefore, the theoretical model with the assumption of $Le = 1$ for the whole region is still able to predict the flame shapes well.

B. Mixed Convective Burning of Two Droplets

The results of local mass flux, mass burning rate, and flame shapes are described here as functions of air velocity and interdroplet separation distance for mixed convective flow around the droplets. For the sake of comparison, the corresponding pure forced convective result is also shown to highlight the effect of buoyancy.

In Figs. 7 and 8, the local mass flux variations along the droplet surfaces have been shown for two different flow velocities and droplet separation distances. Although the local mass flux variation is very similar for both the velocities considered, the effect of separation distance is seen to be very strong; in particular, the local mass flux distribution for the rear droplet is significantly increased in the front portion when the separation distance is increased. This can be attributed to the mixed convective flow bypassing the front portion of the rear droplet for short separation distances, but being able to get more access to that region when the separation is larger. It is observed that the evaporation rates at both the front and rear portions of first droplet are not affected by the variation in separation distance. However, the local mass flux is considerably

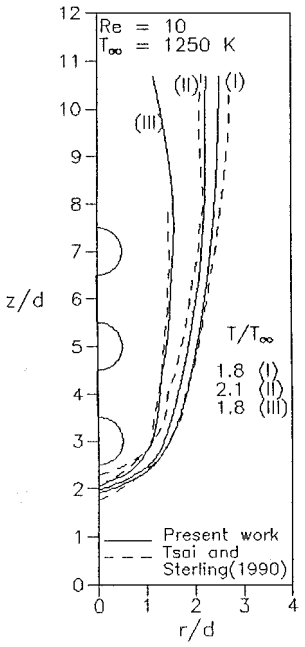

Fig. 5 Isotherms.

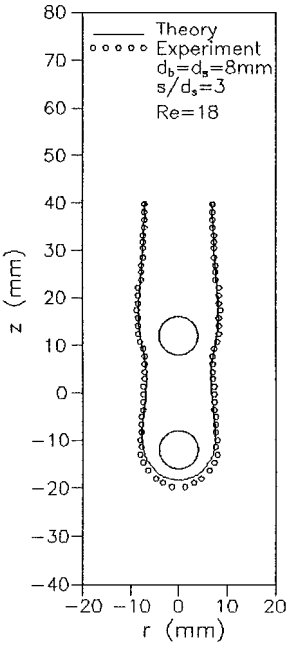

Fig. 6 Flame shape.

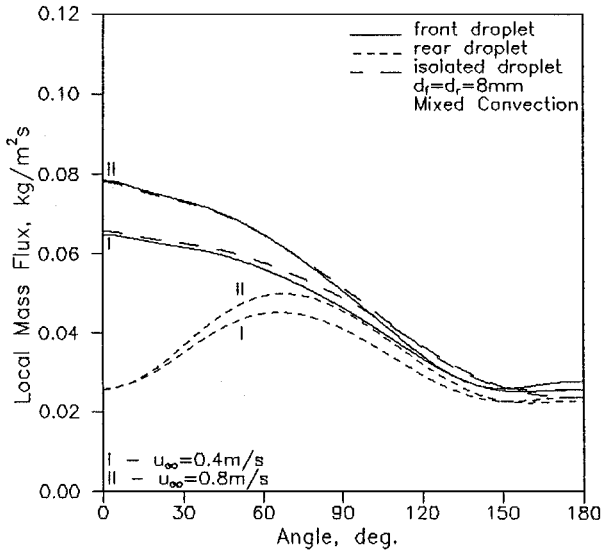

Fig. 7 Variation of local mass flux with respect to angle for different air velocities ($s/d_f = 2$).

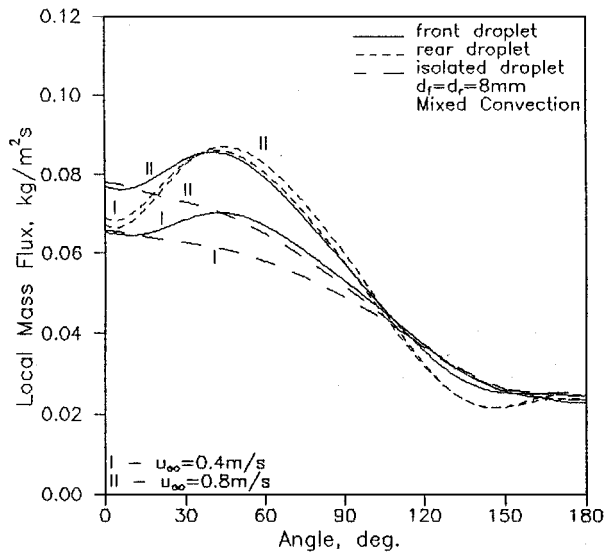

Fig. 8 Variation of local mass flux with respect to angle for different air velocities ($s/d_f = 4$).

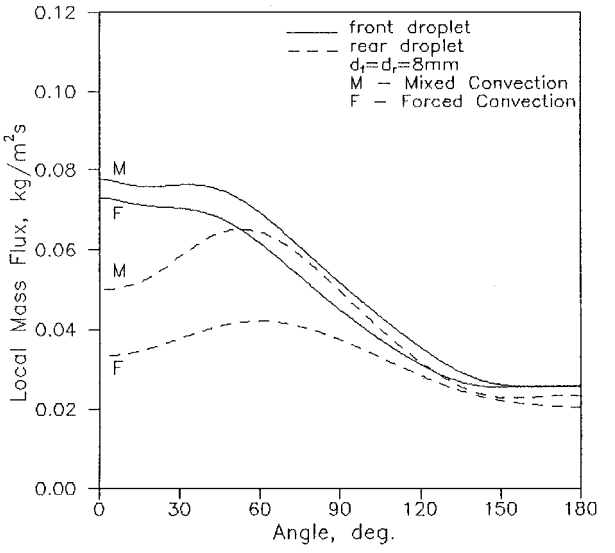

Fig. 9 Variation of local mass flux with respect to angle (equal droplets, $\theta_\infty = 0.8$ m/s, $s/d_f = 3$).

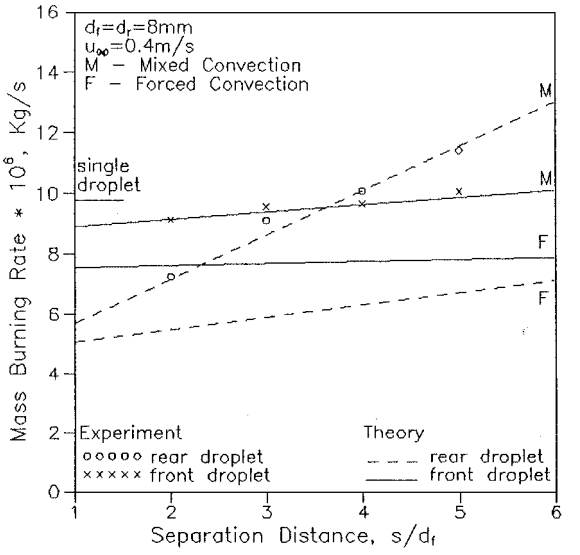

Fig. 10 Variation of mass burning rate with respect to interdroplet separation distance.

affected at around an angle of 45 deg from the front stagnation point for a larger separation distance. This is evidently due to the significant changes in the flow structure around the droplets when the separation distance is increased. For a smaller separation distance ($s/d = 2$), the local mass flux value of the front droplet is essentially equal to that of the isolated droplet. For the rear droplet, the local mass flux increases from a minimum value at the front stagnation point, and, after it reaches a maximum value in the midportion, it decreases again toward the rear stagnation point. Note that this maximum value moves closer to the front stagnation point with an increase in separation distance. The front portion of the rear droplet is very much influenced by the separation distance due to the rising plume from the first droplet, whereas the rear portion is negligibly affected.

In Fig. 9, the mass flux predictions for mixed and forced convection cases are shown for both the droplets. Figure 9 also illustrates that the effect of free convective flow is negligible in the rear portions of both of the droplets and also that the influence is more significant for the rear droplet.

The theoretical and experimental mass burning rate variations with separation distance and air velocity are shown in Figs. 10 and 11. It is observed that the predicted mass burning rates agree

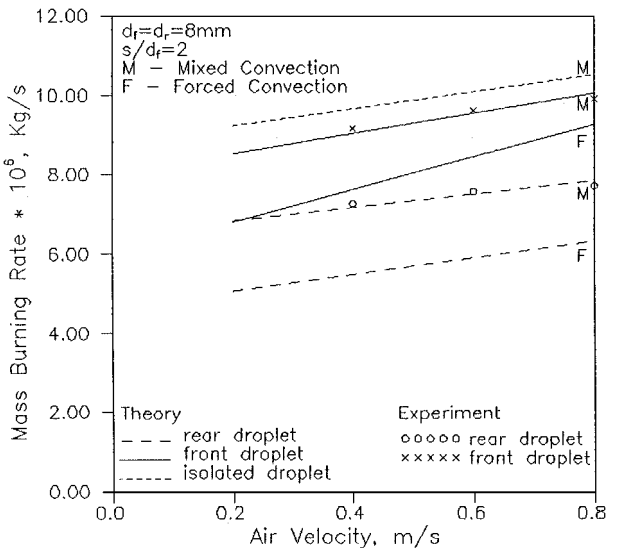

Fig. 11 Variation of mass burning rate with respect to air velocity.

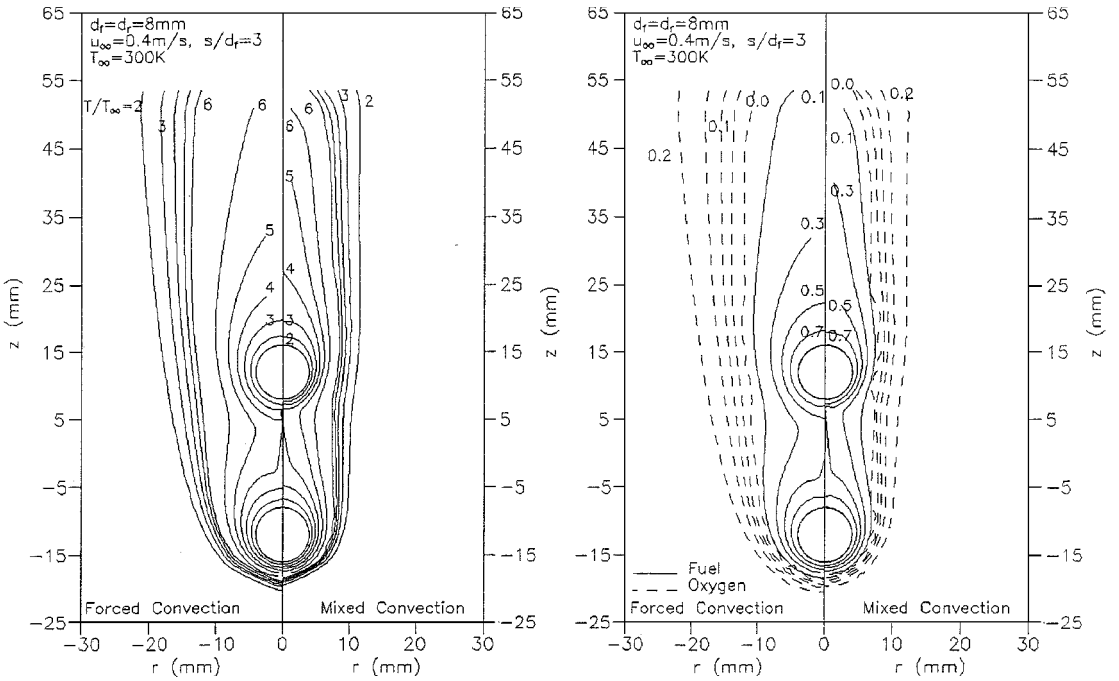

a) Isotherms b) Mass fraction contours

Fig. 12 Predicted profiles for equal droplets.

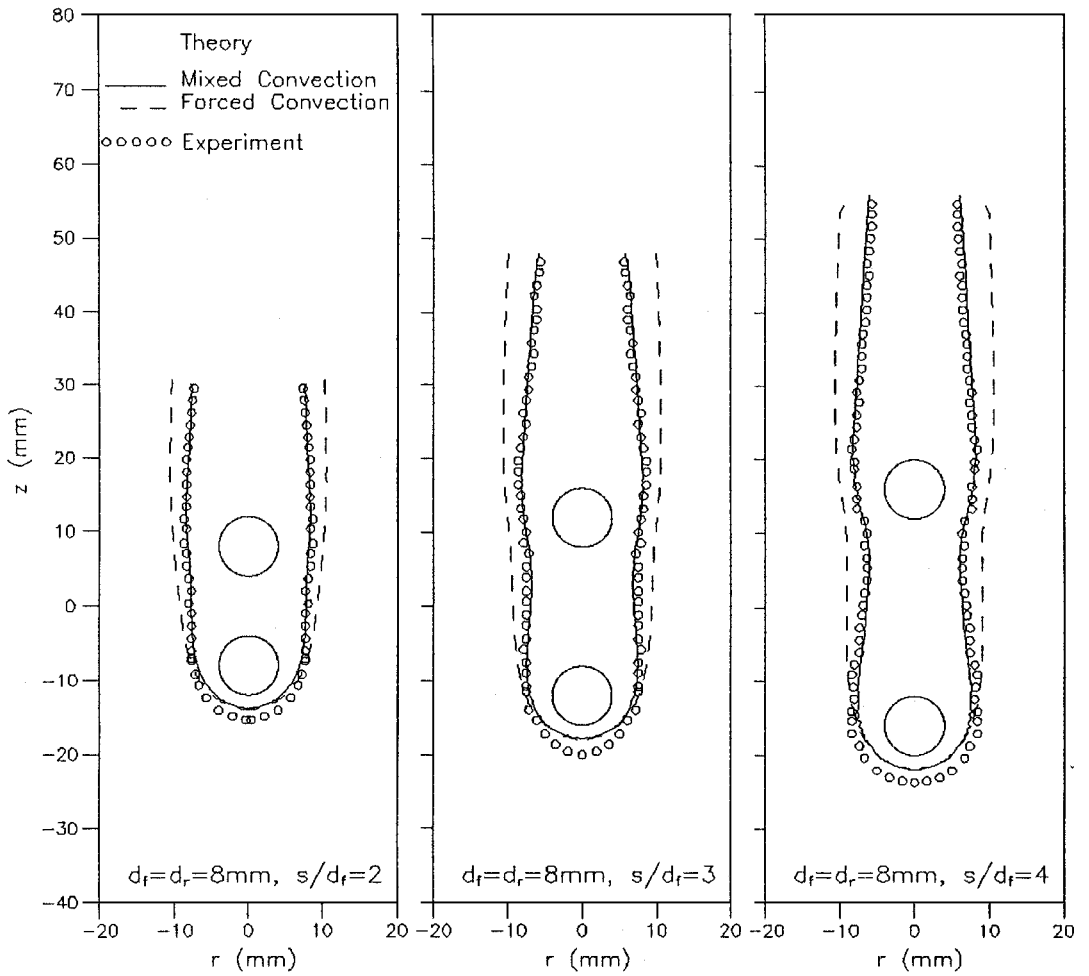

Fig. 13 Flame shapes for different interdroplet distances (fuel: methanol, $\theta_\infty = 0.8$ m/s).

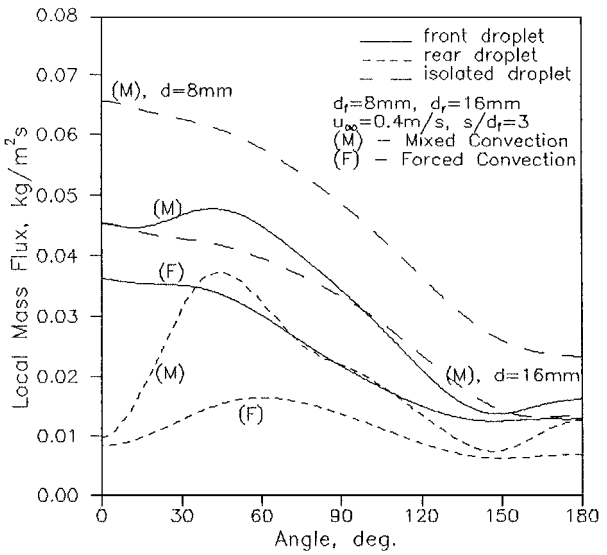

Fig. 14 Variation of local mass flux with respect to angle (smaller droplet in front).

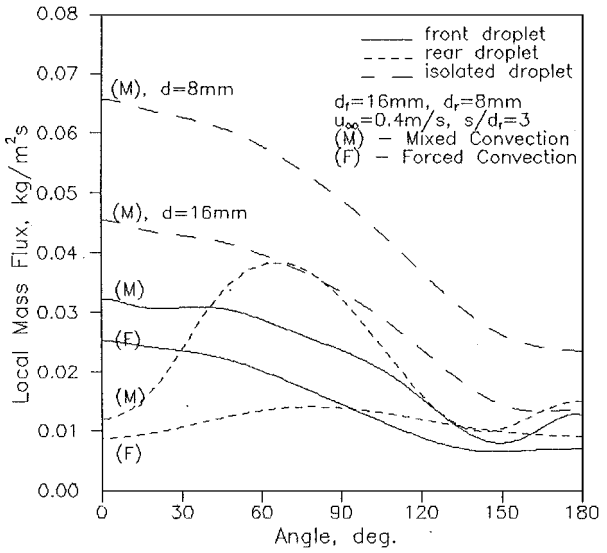

Fig. 15 Variation of local mass flux with respect to angle (bigger droplet in front).

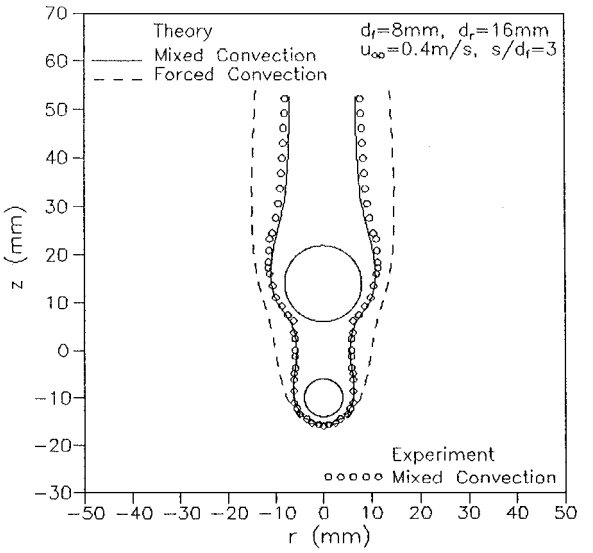

Fig. 16 Flame shapes for unequal droplets (smaller droplet in front).

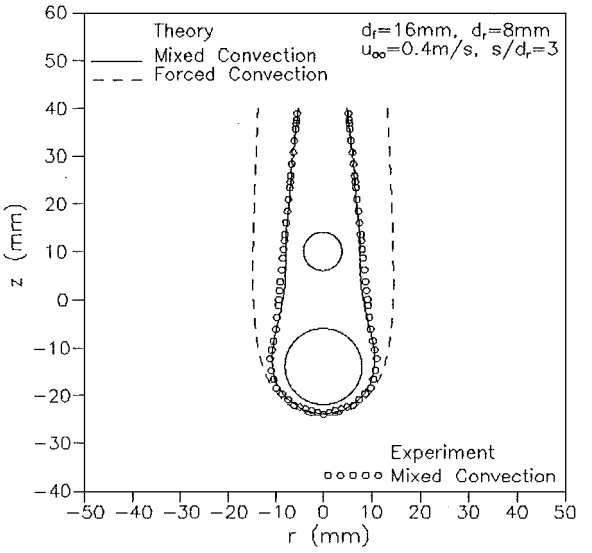

Fig. 17 Flame shapes for unequal droplets (bigger droplet in front).

closely with those measured experimentally. This indicates that the present simplified model provides fairly accurate results. Note from Fig. 10 that in comparison with the rear droplet, the mass burning rate of the front droplet has a weaker variation with the separation distance and that it is closer to that of an isolated droplet (marked in Fig. 10 on the y axis). On the other hand, mass burning rate of the rear droplet decreases by more than a factor of two when s/d is changed from 6 to 1. Note that up to a separation distance of $s/d = 3.5$, the mass burning rate of the rear droplet is less than that of the front droplet. In other words, when the separation distance s/d is more than 3.5, the mass burning rate of the rear droplet is always higher than that of the front droplet until the interaction effects become negligible for very large separation distance values. Also note that at $s/d = 3.5$, the mass burning rates of both the droplets are not only equal, but they are also very close to that of the single droplet. The aforementioned phenomena can be understood better in light of the following observations:

1) At all separation distances, the gaseous mixture surrounding the front droplet is almost similar to that of an isolated droplet because the mixture that approaches the front droplet is fresh. Also, convective effects are very strong over a major portion of the front droplet.

2) Up to the critical separation distance of $s/d = 3.5$, the mass burning rate of the rear droplet is lower than that of the isolated droplet. This is mainly because of the weaker concentration gradients of fuel that exist near the rear droplet due to the flow of unburnt fuel from the first droplet (Fig. 12b).

3) For separation distances higher than $s/d = 3.5$, the rear droplet receives considerable heat from the flame of the front droplet due to better access of the rising plume of the front droplet, and, therefore, it experiences a higher mass burning rate.

For the ranges of parameters considered, the variations of mass burning rate with separation distance and air velocity appear to be approximately linear. From a comparison of the mixed and forced convective results, it is also evident that the effect of buoyancy on mass burning rate increases with s/d, especially for the rear droplet. As regards the effect of air velocity, it is seen that the relative contribution of free convection decreases for the front droplet at higher airflow velocities, whereas for the rear droplet it remains nearly the same.

The theoretically predicted flame shapes are compared with those experimentally obtained for different separation distances as shown in Fig. 13. It is evident that the predicted flame shapes are in reasonable agreement with those obtained from experimental results. At lower separation distances, the flame between the top portion of the front droplet and bottom portion of the rear droplet is shifted away from the axis. This, in turn, decreases the burning rate of the rear droplet. However, as the separation distance increases, a portion of the flame comes closer to the droplet axis, thereby transferring

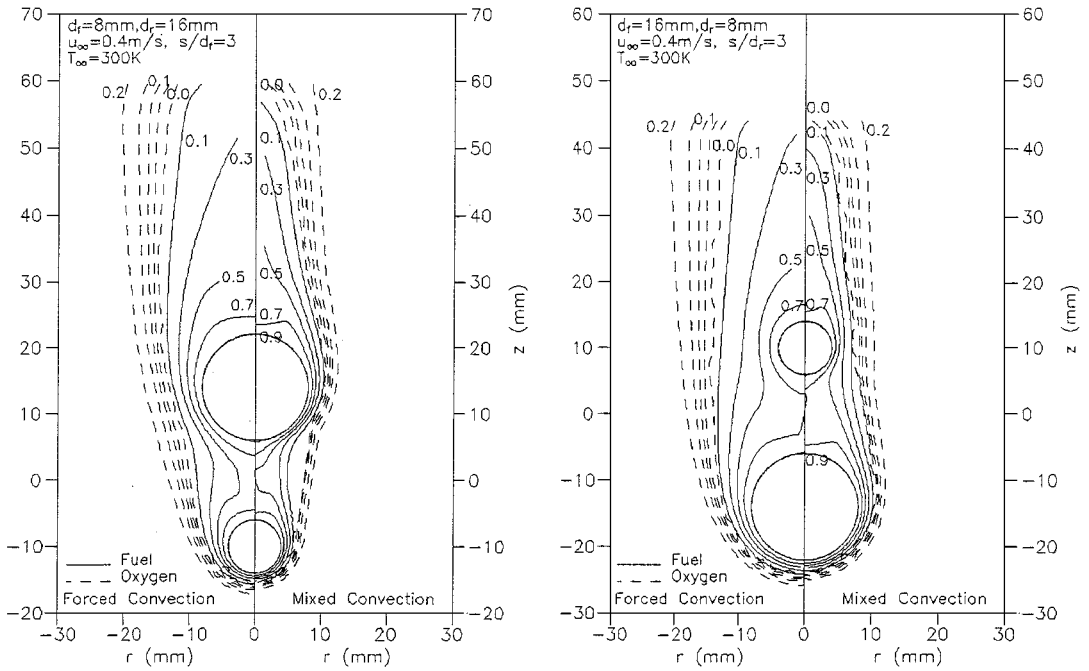

a) Smaller droplet in front **b) Bigger droplet in front**

Fig. 18 Mass fraction contours for unequal droplets.

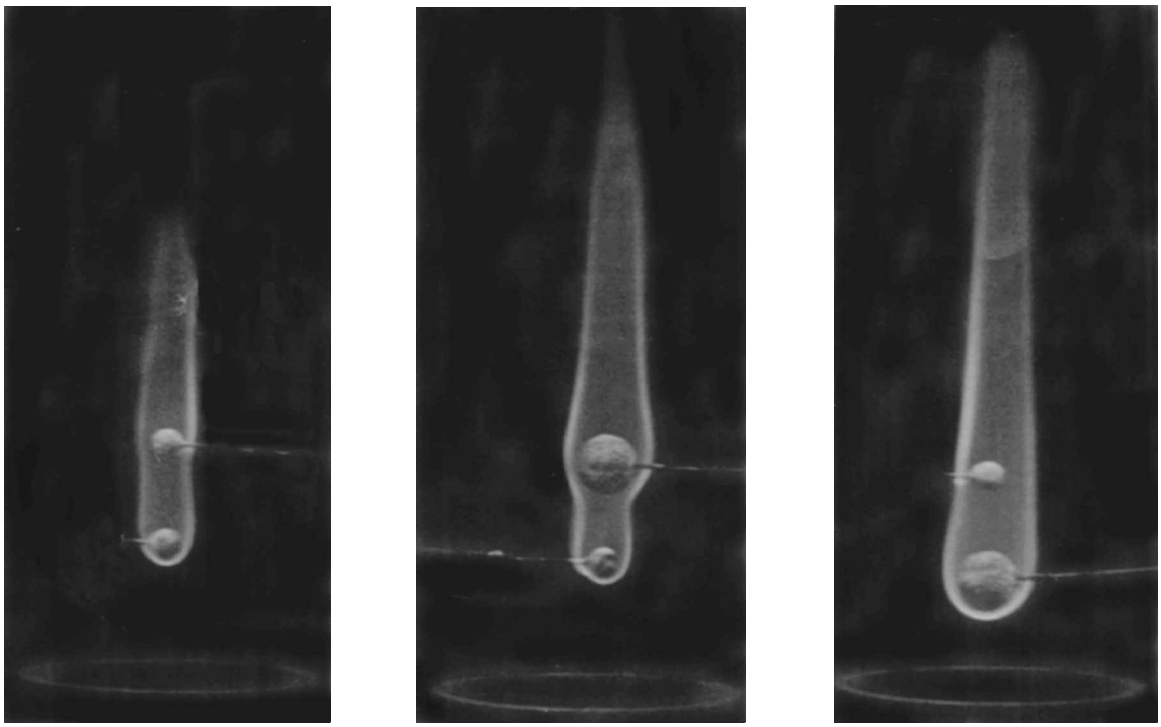

Equal droplets: $d_f = d_r = 8$ mm, $s/d_f = 3$

Smaller droplet in front: $d_f = 8$ mm, $d_r = 16$ mm, $s/d_f = 3$

Bigger droplet in front: $d_f = 16$ mm, $d_r = 8$ mm, $s/d_f = 3$

Fig. 19 Photographs of flame shapes for equal and unequal droplets (upward airflow, $\theta_\infty = 0.4$ m/s).

more heat to the rear droplet. The predictions show that a proper inclusion of the buoyancy term in the governing equation gives rise to good agreement for the flame shape also, when compared with the experimental measurements.

The predicted isotherms and isoconcentration contours for forced and mixed convective cases are plotted in Figs. 12 (on either half of both Figs. 12a and 12b). The maximum temperature predicted is in the range of 1800–2000 K, which is reasonable for hydrocarbon combustion in air. The lateral extent of the heat-affected zone is seen to shrink for the mixed convection case as compared to that for the forced convection case. This may be because of larger velocity values in the thermal plumes rising from the droplets when buoyancy effects are included. The concentration plots also reveal similar features. The isoconcentration curves around the flame surface ($Y_f = Y_o = 0$) show slight oscillations, probably due to loss of numerical accuracy in the extraction of mass fraction from the predicted Shvab–Zeldovich variables near the flame zone.

In Figs. 14–18, the effects of droplet size variation on the combustion process of binary tandem droplets are depicted. The local mass flux distributions shown in Figs. 14 and 15 illustrate that the

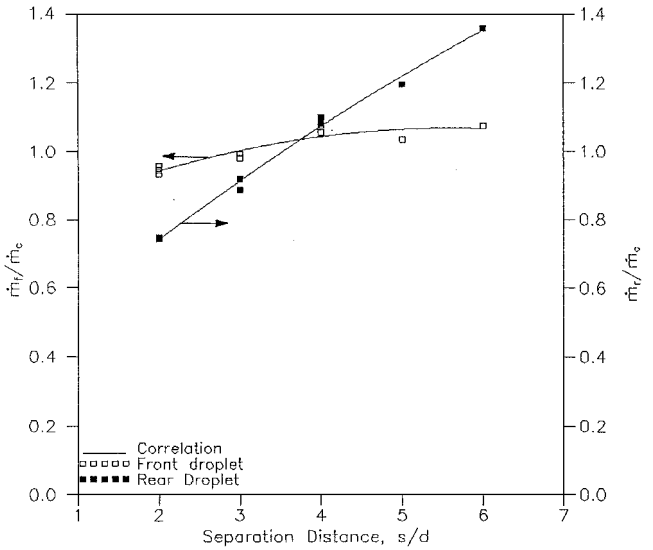

Fig. 20 Mass burning rate correlation for binary droplets burning in tandem arrangement.

mass flux values for both of the droplets are of similar order, and they are less than the evaporation flux for a single droplet when the bigger droplet is in front. When the smaller droplet is in front, the mass flux for the front droplet is more than that for the rear droplet, and it is closer to the isolated droplet value. Also, it is clear that the effects of buoyancy are very strong at the midportion of the rear droplet, regardless of the array configuration. Typical flame photographs obtained for equal and unequal sized droplets are shown in Fig. 19. Comparison of these experimentally obtained shapes with the theoretically predicted ones in Figs. 16. and 17 for the two configurations illustrates that the theoretical model does very well for the cases of unequal droplets also. The difference in flame shape that would arise if buoyancy effects were neglected is also indicated by dotted lines in Figs. 16 and 17. Figure 18 shows the corresponding mass fraction contours for the two droplet configurations. The decrease in the lateral extent of the combustion affected zone for the mixed convective case is evident in these plots also.

C. Mass Burning Rate Correlations

In the preceding section, it was shown that the theoretical predictions for mass burning rates of a binary droplet system are in excellent agreement with the corresponding experimental data for the range of conditions considered in the present study. Here, correlations are presented for the theoretically predicted mass burning rates of equal sized droplets kept in tandem arrangement, in upward air flow (Fig. 20). The mass burning rate for each droplet has been scaled with the mass burning rate of an isolated droplet in a similar convective environment (with the same values of Reynolds and Grashof numbers). Therefore, the quantities $\dot{m}_f/\dot{m}_c$ and $\dot{m}_r/\dot{m}_c$ may be considered as the interaction coefficients for the front and rear droplets, respectively. In Fig. 20, the symbols $\dot{m}_f$, $\dot{m}_r$, and $\dot{m}_c$ denote the mass burning rates of the front, rear, and isolated droplets. The predicted data correlate well in the forms

$$\dot{m}_f/\dot{m}_c = 0.76 + 0.11(s/d) - 0.0096(s/d)^2, \qquad [\pm 3\%] \tag{11}$$

$$\dot{m}_r/\dot{m}_c = 0.36 + 0.20(s/d) - 0.0066(s/d)^2, \qquad [\pm 3\%] \tag{12}$$

in terms of the normalized separation distance s/d. Figure 20 indicates that the burning rate of the front droplet is only mildly different from that of an isolated droplet. Moreover, the interaction coefficient is less than one for s/d less than four and slightly more than one for s/d greater than four. As s/d tends to infinity, the mass burning rate approaches the value corresponding to an isolated droplet. For the rear droplet also, similar trends are observed except that the variation of the interaction coefficient with separation distance is much stronger. The interaction coefficient value being less than one is caused by the flow of unburnt fuel from the first drop, whereas values greater than one can be attributed to greater heat transfer between the two droplets.

VI. Conclusions

A constant property theoretical formulation has been developed and the results have been compared with the experimental data obtained by the use of the porous-sphere technique for the combustion of a tandem droplet array in a mixed convective stream. The theoretical predictions for mass burning rate and flame shape are in excellent agreement with the experimental data obtained. This good agreement of the theoretical model with experiments is attributed to the predominance of convective effects over those of diffusion, for the range of conditions studied. The burning rate of the front droplet is closer to the value for an isolated droplet and it is also a weaker function of separation distance than that for the rear droplet. The present analysis illustrates that the inclusion of density variation in the buoyancy force term in an otherwise constant property formulation can lead to accurate numerical predictions for the combustion of droplets in a mixed convective environment.

Acknowledgment

The first author wishes to express his gratitude to the Department of Atomic Energy for offering the K. S. Krishnan Senior Research Fellowship to pursue the Ph.D. program.

References

[1]Annamalai, K., and Ryan, W., "Interactive Processes in Gasification and Combustion. Part 1: Liquid Drop Arrays and Clouds," *Progress in Energy and Combustion Science*, Vol. 18, No. 3, 1992, pp. 221–295.

[2]Umemura, A., "Interactive Droplet Vaporisation and Combustion: Approach from Asymptotics," *Progress in Energy and Combustion Science*, Vol. 20, No. 4, 1994, pp. 325–372.

[3]Mikami, M., Kato, H., Sato, J., and Kono, M., "Interactive Combustion of Two Droplets in Micro-Gravity," *Twenty-Fifth Symposium (International) on Combustion*, Combustion Inst., Pittsburgh, PA, 1994, pp. 431–438.

[4]Labowsky, M., "A Formalism for Calculating the Evaporation Rates of Rapidly Evaporating Interacting Particles," *Combustion Science and Technology*, Vol. 18, No. 3–4, 1978, pp. 145–151.

[5]Labowsky, M., "Calculation of the Burning Rates of Interacting Fuel Droplets," *Combustion Science and Technology*, Vol. 22, No. 5–6, 1980, pp. 217–226.

[6]Brzustowski, T. A., Twardus, E. M., Wojcicki, S., and Sobiesiak, A., "Interaction of Two Burning Fuel Droplets of Arbitrary Size," *AIAA Journal*, Vol. 17, No. 11, 1979, pp. 1234–1242.

[7]Umemura, A., Ogawa, S., and Oshima, N., "Analysis of the Interaction Between Two Burning Droplets," *Combustion and Flame*, Vol. 41, No. 1, 1981, pp. 45–55.

[8]Williams, A. L., Carstens, J. C., and Zung, J. T., "Drop Interactions in a Spray," *Advances in Chemistry Series*, Vol. 166, 1978, pp. 54–62.

[9]Marberry, M., Ray, A. K., and Leung, K., "Effect of Multiple Particle Interactions on Burning Droplets," *Combustion and Flame*, Vol. 57, No. 3, 1984, pp. 237–245.

[10]Shuen, J. S., "Numerical Study of the Interactions Between Droplets at Intermediate Reynolds Numbers," *Journal of Propulsion and Power*, Vol. 4, No. 6, 1988, pp. 481–489.

[11]Tal, R. T., Lee, D. N., and Sirignano, W. A., "Heat and Momentum Transfer Around a Pair of Spheres in Viscous Flows," *International Journal of Heat and Mass Transfer*, Vol. 27, No. 11, 1984, pp. 1953–1962.

[12]Sirignano, W. A., "The Formulation of Spray Combustion Models: Resolution Compared to Droplet Spacing," *Journal of Heat Transfer*, Vol. 108, No. 3, 1986, pp. 633–639.

[13]Raju, M. S., and Sirignano, W. A., "Interaction Between Two Vaporising Droplets in an Intermediate Reynolds Number Flow," *Physics of Fluids A*, Vol. 2, No. 10, 1990, pp.1780–1796.

[14]Umemura, A., "A Theoretical Study on the Unsteady, Interactive Combustion of a Linear Fuel Droplet Stream," *Twenty-Third Symposium (International) on Combustion*, Combustion Inst., Pittsburgh, PA, 1990, pp. 1445–1453.

[15]Tsai, J. S., and Sterling, A. M., "The Combustion of Linear Droplet Arrays," *Twenty-Third Symposium (International) on Combustion*, Combustion Inst., Pittsburgh, PA, 1990, pp. 1405–1411.

[16]Sivasankaran, K., Seetharamu, K. N., and Natarajan, R., "Numerical Investigation of the Interference Effects Between Two Burning Fuel Spheres," *International Journal of Heat and Mass Transfer*, Vol. 39, No. 18, 1996, pp. 3949–3957.

[17]Roth, N., Anders, K., and Frohn, A., "Mutual Interaction Between Aerosol Droplets in the Micrometer Range," *Journal of Aerosol Science*, Vol. 20, No. 8, 1989, pp. 991–994.

[18]Nguyen, Q. V., Rangel, R. H., and Dunn-Rankin, D., "Measurement and Prediction of Trajectories and Collision of Droplets," *International Journal of Multiphase Flow*, Vol. 17, No. 2, 1991, pp. 159–177.

[19]Kassoy, D. R., and Williams, F. A., "Variable Property Effects on Liquid Droplet Combustion," *AIAA Journal*, Vol. 6, No. 10, 1968, pp. 1961–1965.

[20]Law, C. K., and Law, H. K., "Quasi-Steady Diffusion Flame Theory with Variable Specific Heats and Transport Coefficients," *Combustion Science and Technology*, Vol. 12, No. 4–6, 1976, pp. 207–216.

[21]Kuo, K. K., *Principles of Combustion*, Wiley, New York, 1986, pp. 210–214.

[22]Taylor, C., and Hughes, T. G., *Finite Element Programming of the Navier–Stokes Equations*, Pineridge, Swansea, Wales, U.K., 1981, pp. 120–130.

J. R. Bellan
Associate Editor